SCIENTIFIC REPORTS

OPEN

SUBJECT AREAS:
OPTICAL SPECTROSCOPY
MEMBRANE STRUCTURE AND ASSEMBLY
INTEGRINS
MEMBRANE PROTEINS

Received
18 September 2014

Accepted
16 December 2014

Published
19 January 2015

Correspondence and requests for materials should be addressed to L.Z. (zlhustc@ustc.edu.cn) or C.T. (cltian@ustc.edu.cn)

* These authors contributed equally to this work.

CW-EPR studies revealed different motional properties and oligomeric states of the integrin β_{1a} transmembrane domain in detergent micelles or liposomes

Lu Yu[1,2]*, Wei Wang[1]*, Shenglong Ling[1], Sanling Liu[2], Liang Xiao[1], Yanlong Xin[1], Chaohua Lai[1], Ying Xiong[1], Longhua Zhang[1] & Changlin Tian[1,2]

[1]Hefei National Laboratory of Microscale Physical Sciences, School of Life Sciences, University of Science and Technology of China, Hefei, Anhui, 230027, P. R. China, [2]High Magnetic Field Laboratory, Hefei institutes of Physical Science, Chinese Academy of Sciences, Hefei, Anhui, 230031, P. R. China.

Integrins are heterodimeric membrane proteins that regulate essential processes: cell migration, cell growth, extracellular matrix assembly and tumor metastasis. Each integrin α or β subunit contains a large extracellular domain, a single transmembrane (TM) domain, and a short cytoplasmic tail. The integrin TM domains are important for heterodimeric association and dissociation during the conversion from inactive to active states. Moreover, integrin clustering occurs by homo-oligomeric interactions between the TM helices. Here, the transmembrane and cytoplasmic (TMC) domains of integrin β_{1a} were overexpressed, and the protein was purified in detergent micelles and/or reconstituted in liposomes. To investigate the TM domain conformational properties of integrin β_{1a}, 26 consecutive single cysteine mutants were generated for site-directed spin labeling and continuous-wave electron paramagnetic resonance (CW-EPR) mobility and accessibility analyses. The mobility analysis identified two integrin β_{1a}-TM regions with different motional properties in micelles and a non-continuous integrin β_{1a}-TM helix with high immobility in liposomes. The accessibility analysis verified the TM range (Val737-Lys752) of the integrin β_{1a}-TMC in micelles. Further mobility and accessibility comparisons of the integrin β_{1a}-TMC domains in micelles or liposomes identified distinctively different oligomeric states of integrin β_{1a}-TM, namely a monomer embedded in detergent micelles and leucine-zipper-like homo-oligomeric clusters in liposomes.

Integrins constitute a large family of heterodimeric adhesion receptors that regulate essential processes associated with cell-cell and cell-matrix interactions such as cell migration, cell growth, extracellular matrix assembly and tumor metastasis[1,2]. Each integrin consists of an α and a β subunit, both of which contain a relatively large extracellular domain, a single transmembrane domain (TM), and a short cytoplasmic tail[3]. In humans, 18 α and 8 β subunits combine to form different integrins[4]. The TM domains of the integrin α and β subunits play critical roles in bidirectional signal transduction across the plasma membrane[5–7]. A series of mutational studies showed that a specific TM helix-helix packing in the integrin $\alpha_{IIb}\beta_3$ dimer represents the inactive state, whereas disruption of the inter-helical interaction activates signal transduction[5,6]. Specifically, the inactive integrin $\alpha_{IIb}\beta_3$ state is stabilized by the hydrophobic heterodimerization packing of the TM helices and electrostatic interactions in the TM and adjacent cytoplasmic regions, whereas integrin activation ensues from the separation of the TM domains[7–10]. Recent studies reported the formation of an active receptor cluster with inter-helical interactions between TM domains of homo-oligomeric integrins after ligand binding (Fig. 1a)[11]. The active integrin clusters were detected in many cell types and shown to localize to cell- extracellular matrix (ECM) contacts[12]. The integrin cluster forms the basis for cell-ECM adhesion complexes that transfer force between the cell and the ECM and facilitate intracellular signaling, leading to protein phosphorylation and cytoskeletal attachment[12,13].

Among the different β subunits, β_1 integrin is the most abundantly expressed in adhesion-dependent cells[14]. The β_1 integrin subunit can associate with at least 10 different α subunits to form distinct integrin heterodimers

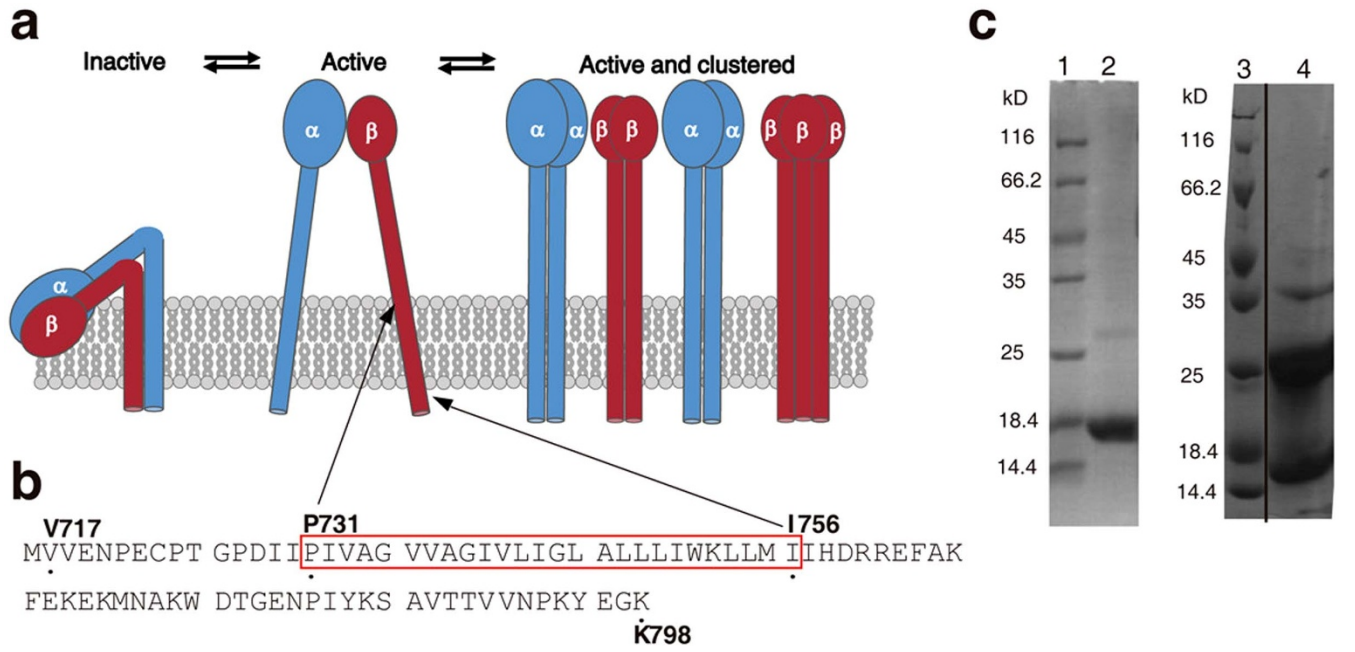

Figure 1 | (a) Integrin architecture and potential mechanism for the activation and clustering of integrins. Specific contacts between the ectodomains, the TMH, and cytoplasmic domains keep the integrin α (blue) and β (red) subunits proximal in the inactive state. Concomitant with activation, the transmembrane domains become separated and available for homomeric interactions. Homomeric association of the transmembrane domains leads to clustering on the cell surface[11]. (b) Primary sequence of the integrin β_{1a}-TMC domain depicted with starting and ending residue numbers (V717 and K798). Residues selected for site-directed spin labeling one at a time (P731 to I756) are highlighted by framing in red. (c) SDS-PAGE analysis of integrin β_{1a}-TMC in detergent micelles (left gel) and lipid liposomes (right gel). Lane 1 and lane 3 are molecular size markers. Lane 2 is integrin β_{1a} variant L747C in detergent micelles while lane 4 is the variant L749C in lipid liposomes. L747C in detergent micelles migrated with a molecular weight of approximately 16 kDa as a monomer, while L749C in lipid liposomes migrated as multiple-bands of monomers, dimers and trimers. The gels have been run under the same experimental conditions and were cropped to improve the clarity and conciseness of the presentation. A vertical dividing line was drawn at the splice junction to show non-adjacent lanes in the SDS-PAGE for samples in lipid liposomes. Full-length gels are presented in Supplementary Figure S1.

capable of interacting with various extracellular matrix molecules as well as some cell adhesion molecules[14]. A subgroup of collagen integrin receptors, namely α_1/β_1, α_{10}/β_1 and α_{11}/β_1, were found to mediate cell adhesion to the ECM[15]. Among them, integrin α_1/β_1 plays a role in fibrosis regulation[16], cancer-related angiogenesis[17], chronic inflammation[18], the development of myopia[19], and in the homing and differentiation of prostate cancer stem cells[20]. The transmembrane domain and cytoplasmic tails of most β subunits show significant sequence homology[21,22]. Several structural and functional studies have analyzed the transmembrane domain (or cytoplasmic tail) of several integrin proteins, such as integrin α_{1a}, α_{IIb}/β_3, β_{1d} and β_3, using solution NMR methods[23–26]. However, no detailed reports focusing on the structural and biophysical characterization of integrin β_{1a} have been published to date.

In the last decades, site-directed spin labeling (SDSL) electron paramagnetic resonance (EPR) spectroscopy has emerged as an effective method to study structural details, dynamics and conformational transitions of spin-labeled membrane proteins, especially in lipid bilayers[27], or detergent micelles (a liposome mimic)[28]. In protein EPR studies, an unpaired electron is introduced by site-directed spin labeling of methanethiosulfonate (MTSL, R1) at a specific site through disulfide bond formation with a cysteine mutated from the native residue[29]. Acquired EPR signals of the introduced R1 groups can provide detailed information on side chain dynamics, polarity and topology profiles across the membrane lipid bilayer, as well as the distances between two spin labeled residues[30]. Unlike X-ray crystallography or solution NMR[31,32], the high resolution three dimensional structure of membrane proteins is difficult to obtain by EPR. However, the combination of SDSL and EPR can provide dynamic and topological per residue information of membrane proteins in the presence of detergent micelles or liposomes. The higher gyromagnetic (γ) constant of electrons compared to that of nuclei (^{1}H, ^{13}C, ^{15}N) guarantees an approximately 1000× sensitivity gain in EPR from that of NMR in protein dynamics studies, especially for eukaryotic membrane proteins, whose overexpression cannot be achieved in bacterial systems, or in isotope incorporation, which cannot be implemented in eukaryotic cell culture.

Here, the integrin β_{1a} transmembrane domain and cytoplasmic tail (TMC) were overexpressed and purified in detergent micelles, and reconstituted in liposomes. A series of cysteine mutations were introduced in the integrin β_{1a}-transmembrane helix (TMH) domain for spin radical labeling (Fig. 1b). Then, SDSL-EPR was used to examine the structural and dynamic properties of the integrin β_{1a}-TMH in detergent micelles or liposomes, using EPR line-shape analysis and accessibility estimation in the presence of paramagnetic regents (hydrophobic O_2 or hydrophilic NiEDDA)[33]. The observed differences in dynamics or topology between the integrin β_{1a}-TMC in detergent micelles and in liposomes suggested the presence of a monomeric integrin β_{1a}-TMH in detergent micelles and homo-oligomers of the protein in liposomes, which could be attributed to leucine-zipper-like inter-helical interactions.

Results

The integrin β_{1a}-TMC forms homo-oligomers in liposomes. The integrin β_{1a}-TMC was overexpressed as inclusion bodies in *E. coli*. The protein was refolded and purified in buffers containing LDAO micelles after Ni^{2+}-NTA affinity chromatography. Size exclusion chromatography was used for further protein purification. SDS-PAGE was used to further characterize protein purity and oligomeric states. A single band at approximately 16 kDa was observed in the sample of integrin β_{1a}-TMC in LDAO micelles (Fig. 1c left). The observed molecular weight from SDS-PAGE was higher than the

theoretical value of 10.3 kD (91 amino acids) for the integrin β_{1a}-TMC. The slower migration rate in SDS-PAGE was possibly due to the strong interaction between the hydrophobic TMH and the detergents, resulting in a non-denatured state and a larger size than that of the pure protein[34]. To verify the lowest possible molecular weight of the band, the sample was boiled intensively before loading onto SDS-PAGE; however, no bands of smaller size (or faster migration rate) were observed (data not shown). These findings suggested that the protein existed as a monomer in micelles. More than three bands were observed for the sample containing the integrin β_{1a}-TMC reconstituted in POPC/POPG liposomes (Fig. 1c right). These bands were 16, 26, and 37 kDa. The molecular weight differences derived from the SDS-PAGE bands were approximately 10 kDa and 11 kDa, which was consistent with the net protein size of the integrin β_{1a}-TMC (10.3 kDa). This observation suggested that the 16 kDa band was the monomeric form of integrin β_{1a}-TMC. At the same time, the detection of a series of protein bands by SDS-PAGE indicated the presence of homo-oligomeric integrin β_{1a}-TMC, and was evidence of strong inter-monomeric interactions (not disrupted in harsh detergent like SDS). The 16, 26 and 37 kDa bands possibly represented the monomer, dimer and trimer forms of the integrin β_{1a}-TMC after reconstitution in liposomes. Several previous studies reported the presence of homo-oligomeric integrin protein clusters in the cell membrane, especially during cell metastasis[35,36]. However, the detailed mechanism driving the formation of integrin homo-oligomers remains to be elucidated.

Circular dichroism (CD) spectroscopy was used to estimate the secondary structure of the integrin β_{1a}-TMC in detergent micelles (Supplementary. Fig. S2). No CD data of the protein in liposomes were obtained because of the large size of proteoliposomes and the consequent light scattering. Approximately 40% of the α-helical contents were derived from the CD data of the protein in LDAO micelles, which was consistent with the secondary structure prediction of the integrin β_{1a}-TMC, namely a helical transmembrane domain and a random coil cytoplasmic tail. At the same time, high sequence homology was observed among integrins β_{1a}, β_{1d} and β_3 (Supplementary. Fig. S3), especially the conserved residues in the transmembrane domains. The solution NMR structure of β_{1d} and β_3 demonstrated the helical secondary structure in the transmembrane domain[23,26]. Taken together, these findings suggested that the transmembrane domain of integrin β_{1a}-TMC adopted the helical secondary structure.

CW-EPR spectra of the transmembrane residues of integrin β_{1a}-TMC in LDAO micelles or POPC/POPG liposomes. After the mutation of cysteine residues in each site of the integrin β_{1a}-TMH domain (from P731-I756), spin radical probe MTSL was performed in each cysteine site through disulfide bond formation of the purified integrin β_{1a}-TMC in LDAO micelles, and the protein was then reconstituted in POPC/POPG liposomes. CW-EPR spectra were acquired for a total of 52 samples (26 each) of MTSL-labeled integrin β_{1a}-TMC in LDAO micelles (Fig. 2a) or POPC/POPG liposomes (Fig. 2b) at ambient temperature (298 K).

As shown in Figure 2a, all CW-EPR spectra of integrin β_{1a}-TMC in LDAO micelles showed conventional three line spectra, with single values reflecting splitting of the hyperfine extrema $2A'_{zz}$ (between $m_{i=-1}$ and $m_{i=+1}$), which indicated mono-dispersion of the conformational and motional properties of each residue in the integrin β_{1a}-TMH in LDAO micelles. Overall broadening of spectral lines was observed in the CW-EPR spectra of integrin β_{1a}-TMC in liposomes (Fig. 2b), indicating that the dynamic motion of the nitroxide spin-label was slower in liposomes than in micelles. Moreover, CW-EPR spectra with two populations of $2A'_{zz}$ splitting were observed for some sites of integrin β_{1a}-TMC in POPC/POPG liposomes at positions A746, L748, L749, I750, L753, L754 and M755 (* labeled in Figure 2b). This strongly indicated the presence of both immobilized (i) and mobilized (m) components at these sites. The two motional components detected in the EPR spectra suggested the presence of two different motional or conformational states of these residues of integrin β_{1a}-TMC in liposomes.

Mobility analysis of the transmembrane residues of integrin β_{1a}-TMC in LDAO micelles or POPC/POPG liposomes. The acquired EPR spectra permitted derivation of the rotational correlation time (τ_c) by empirical estimation[37,38]. The estimated τ_c values for several selected residues (G735R1, I740R1, G744R1, L749R1 and M755R1) of integrin β_{1a}-TMC in detergent micelles and in liposomes are shown in Figure 3. For each residue, the rotational correlation time was longer in liposomes than in detergent micelles, consistent with the overall immobilization in liposomes, as revealed by spectral line broadening (Fig. 2). Furthermore, for residues of integrin β_{1a}-TMC with two different dynamic components in liposomes (L749R1 and M755R1), the rotational correlation times corresponding to "mobile" and "immobile" components were quantified. The "immobile" component, with τ_c values of up to 20–40 nanoseconds, reflected a heavily restricted dynamic state of R1, which might have resulted from the interactions between the specific residue and other residues or lipid molecules.

The inverse line width of the central $m_{I=0}$ resonance line (ΔH^{-1}) and the inverse spectral second moment ($<H^2>^{-1}$) are normally used as comprehensive descriptors of nitroxide mobility and the corresponding structural features[39], which may quantitatively reflect the motional modes of MTSL labeled sites in a semi-empirical way. Here, ΔH^{-1} and $<H^2>^{-1}$ were analyzed to further extract information on the mobility of the integrin β_{1a}-TMC in detergent micelles and in liposomes (Fig. 4).

For the samples of integrin β_{1a}-TMC in LDAO micelles, the maximum and minimum motional τ_c values of the 26 MTSL labeled sites were 2.09 ns (L754R1) and 1.83 ns (G735R1), respectively. Theoretically, the periodic intensity oscillation of the ΔH^{-1} and $<H^2>^{-1}$ values in stretches of a protein segment reflect the secondary structure of the protein because of the heterogeneity of its local environment[39]. Here, no such obvious intensity oscillation periodicity was observed for the sample in LDAO micelles; however, the ΔH^{-1} (Fig. 4a, black squared data) decreased progressively from the N-terminus to the C-terminus residues of the transmembrane domain. The observed non-periodicity of the two mobility descriptors was consistent with a monomeric integrin β_{1a}-TMC surrounded by detergent micelles, which provided only residue-detergent interactions and should be more homogeneous than the diverse inter-residue interactions in local tertiary cavities of soluble proteins[40]. Almost constant or slightly increasing $<H^2>^{-1}$ values were observed from P731R1 to G744R1, whereas decreasing $<H^2>^{-1}$ values after G744R1 indicated a higher degree of immobility for residues from L745R1 to I756R1 (Fig. 4b, black squared data). Splitting of the outer hyperfine extrema ($2A'_{zz}$), which is also a measure mobility, showed similar pattern of change (Supplementary. Fig. S4, black squared data). The correlation diagram of ΔH^{-1} and $<H^2>^{-1}$ directly reflected the mobility distributions of residues in the integrin β_{1a}-TMH domain. Two distinct regions were observed for samples in LDAO micelles (Fig. 4c): the residues from P735R1 to G744R1 were more mobile than the residues from L745R1 to I756R1, indicating the presence of two regions in the integrin β_{1a}-TMH domain. The N-terminal segment was more mobile than the C-terminal segment, which could be attributed to the presence of three Gly and one Pro residues in the N-terminus compared to more Leu and Ile residues in the C-terminal region. Strong hydrophobic interactions between the Leu or Ile residues in the C-terminal region and the core of detergent micelles may have resulted in the relatively lower mobility.

For the sample of integrin β_{1a}-TMC in POPC/POPG liposomes, large mobility variations were derived from the EPR spectra due to

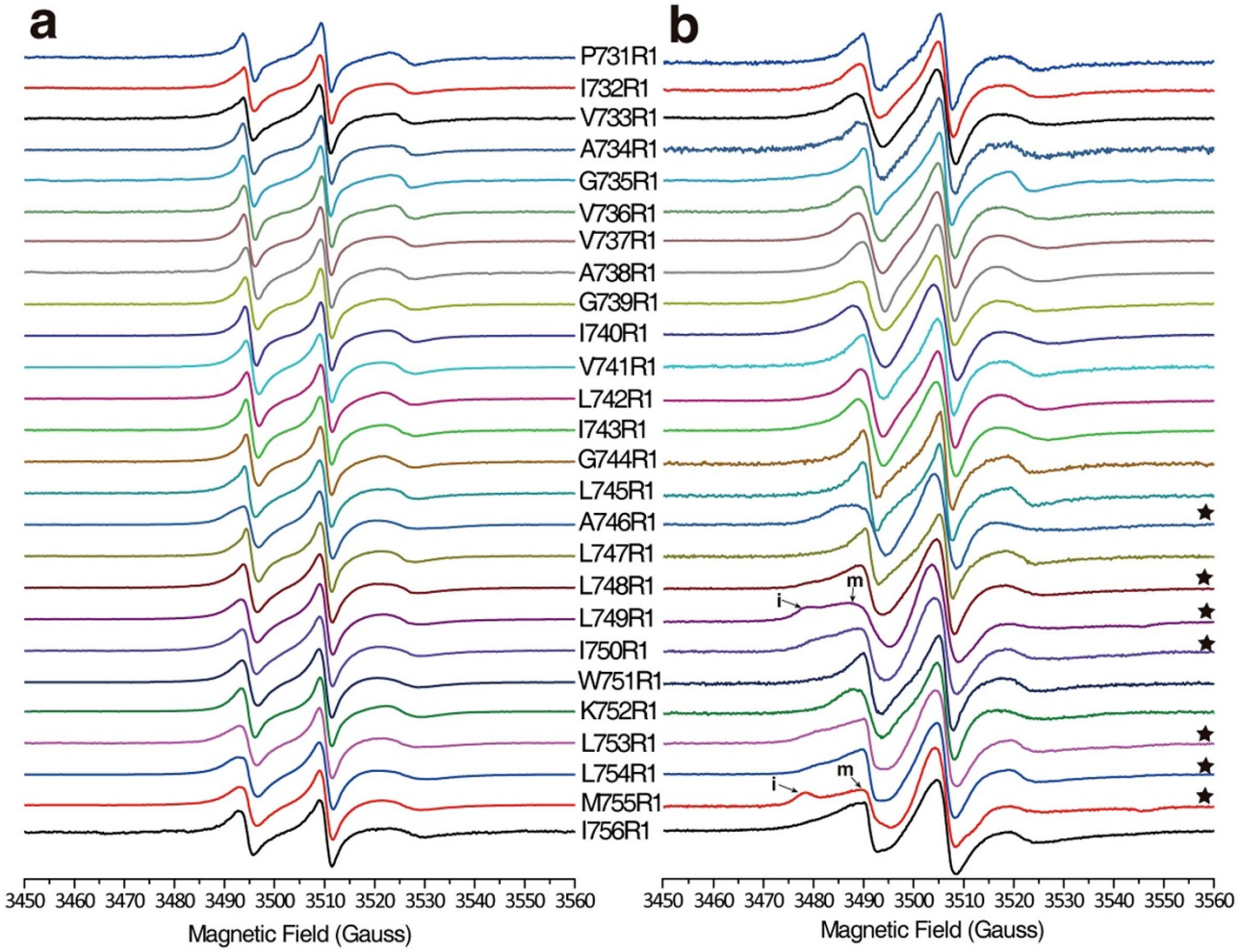

Figure 2 | EPR spectra of spin-labeled integrin β_{1a}-TMC scanning the transmembrane region P731–I756. (a) EPR spectra of integrin β_{1a}-TMC in LDAO micelles. (b) EPR spectra of integrin β_{1a}-TMC reconstituted in POPC/POPG liposomes. Each spectrum was normalized by the height of the central peak. Asterisks indicate spectra that exhibit multiple components in lipid liposomes. "i" and "m" represent the "immobile" and "mobile" components, respectively, on the spectra of L749R1 and M755R1.

the presence of both mobile and immobile components of some residues in the TM domain (Fig. 2b). Both the ΔH^{-1} and $<H^2>^{-1}$ values derived from the EPR spectra showed high amplitude fluctuations (Fig. 4a and Fig. 4b, red dots data). The fit of the sine-wave, with a periodicity of 3.6 (α-helix), with the ΔH^{-1} and $<H^2>^{-1}$ values in two segments (P731R1-I743R1; L745R1-K752R1) indicated that the two segments adopted an α-helical secondary structure with the junction at G744. Periodic oscillation was also observed for $2A'_{zz}$ values of integrin β_{1a}-TMC in POPC/POPG liposomes (Supplementary. Fig. S4, red dots data). At the same time, the observed periodicity strongly implied the presence of inter-residue steric interactions in the sample of integrin β_{1a}-TMC in POPC/POPG liposomes, which was consistent with the previously observed oligomeric bands in the SDS-PAGE analysis of integrin β_{1a}-TMC in liposomes (Fig. 1c right). Under these conditions, the sites with lower mobility were mapped to V733R1, V737R1, I740R1, I743R1, A746R1, L749R1, L753R1, and L754R1. Among the residues with low ΔH^{-1} and $<H^2>^{-1}$ values, the L749R1, L753R1, L754R1 sites were found to have immobile components in the EPR spectra (Fig. 2b, marked with an asterisk). In the proposed homo-oligomers of integrin β_{1a}-TMC in liposomes, these Leu sites could play major roles in inter-helical interactions, such as those found in the Leucine zipper domain[41,42].

The ΔH^{-1} (Fig. 4a) and $<H^2>^{-1}$ (Fig. 4b) values and the $\Delta H^{-1} \sim <H^2>^{-1}$ correlation diagram (Fig. 4d) were compared between samples of integrin β_{1a}-TMC in LDAO micelles and in POPC/POPG liposomes. As described above, smaller values but much larger fluctuations of ΔH^{-1} and $<H^2>^{-1}$ were observed for the protein in liposomes than in detergent micelles, indicating decreased motion of the sites of the integrin β_{1a}-TMC in liposomes. This was further verified by the correlation diagram in Figure 4d. The highly immobilized sites were likely due to the inter-reside interactions in the homo-oligomeric integrin β_{1a}-TMC in liposomes compared to the residue-detergent interactions for monomeric integrin β_{1a}-TMC in detergent micelles.

Accessibility analysis of the integrin β_{1a}-TMH in LDAO micelles or POPC/POPG liposomes. For membrane protein topology analysis, the accessibility of protein side chains provides valuable information[30]. In EPR studies, the solvent accessibility of R1 in a membrane protein can be inferred from the collision frequency of the nitroxide radical probe with paramagnetic relaxing reagents in aqueous solution or in a hydrophobic environment. Normally, both molecular oxygen (O_2) and 50 mM NiEDDA are applied for accessibility analysis of R1[33]. The nonpolar molecule oxygen (O_2) is more soluble in the hydrophobic interior of membranes or micelles than in aqueous solution. At the same time, the polar reagent NiEDDA shows high solubility in aqueous solution and low solubility in hydrophobic media. Therefore, the accessibility parameter (Π) is proportional to the collision frequency of

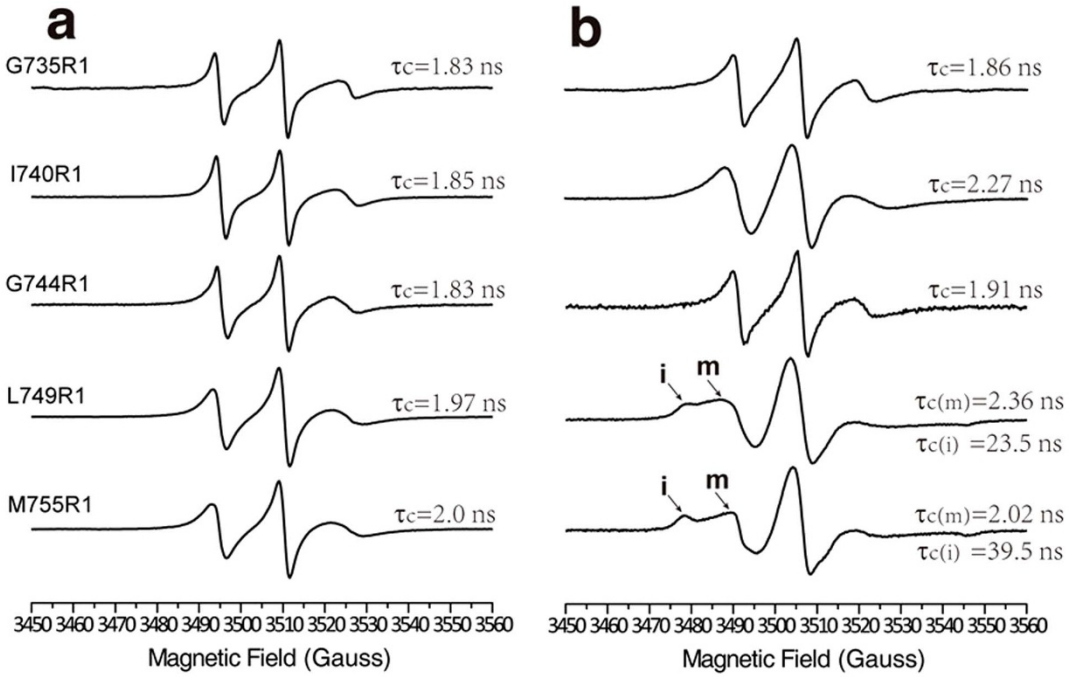

Figure 3 | Rotational correlation time (τ_c) estimation of integrin β_{1a}-G735R1, -I740R1, -G744R1, -L749R1 and -M755R1 collected at 298K in LDAO micelles (a) and in POPC/POPG liposomes (b). Rotational correlation times are shown beside each spectrum. For integrin β_{1a}-L749R1 and β_{1a}-M755R1, two different motional components were observed. The ''immobile'' and ''mobile'' components were represented by ''i'' and ''m'', respectively and the corresponding rotational correlation times (τ_c) are shown.

nitroxide with either O_2 or NiEDDA, which can be estimated using power saturation EPR techniques[33]. The conjugated accessibility analysis using Π_{O2} and Π_{NiEDDA} can provide detailed information on protein-lipid interactions, especially in the junctional residues between the hydrophobic and hydrophilic regions. In the present study, both Π_{O2} and Π_{NiEDDA} for R1 labeled in the transmembrane sites (P731–I756) of integrin β_{1a}-TMC were collected for integrin β_{1a}-TMH topology analysis using power saturation EPR methods. Figure 5 shows the recorded saturation curves for selected residues (V733R1, V741R1, A746R1 and M755R1) of the integrin β_{1a}-TMC in detergent micelles and in liposomes after exposure to the paramagnetic relaxing reagent O_2 or NiEDDA (N_2 was used as a control). The Π_{O2} and Π_{NiEDDA} values for each residue derived from fitting the saturation curves are shown in Figure 5. The derived Π_{O2} and Π_{NiEDDA} values for all 26 residues of the integrin β_{1a}-TMH in detergent micelles and in liposomes are shown in Figure 6.

For the sample of integrin β_{1a}-TMC in LDAO micelles, the results of accessibility analysis of O_2 and NiEDDA are shown in Figure 6a and 6b (black squared data), respectively. Correlational analysis of the conjugated Π_{O2} and Π_{NiEDDA} values can provide topology information of the transmembrane sites labeled with spin radical R1. In Figure 6a, the Π_{NiEDDA} values decreased progressively from the V733R1 site to the A738R1 site, indicating a lower accessibility of these sites to the hydrophilic NiEDDA compound. Then, a series of low Π_{NiEDDA} values from A738R1 to W751R1, suggested that these sites were in a less hydrophilic region. The Π_{NiEDDA} values increased from the W751R1 site to the end point at I756R1. The Π_{O2} values shown in Figure 6b also showed two levels of distribution, namely low values between P731R1 and V736R1 and between K752R1 and I756R1; and high values between A738R1 and W751R1. With the two conjugated properties of O_2 and NiEDDA, the function $\Phi = \ln[\Pi_{O2}/\Pi_{NiEDDA}]$ was normally applied to reduce the effect of steric factors and to provide a value proportional to the simple concentration ratio of the paramagnetic reagents in the immediate environment of R1[33]. Thus, Φ could be at or near a local maximum for sites exposed to the hydrophobic interior, whereas low values were maintained at the interfacial regions proximal to the aqueous solvent. The calculated $\Phi_{micelle}$ values for integrin β_{1a}-TMC in LDAO micelles are shown in Figure 6c (black squared data) and the $\Phi_{micelle}$ values showed a similar pattern to that of the Π_{O2} values. Therefore, the $\Phi_{micelle}$ values and the conjugated Π_{O2} and Π_{NiEDDA} values of integrin β_{1a}-TMC in LDAO micelles indicated a standard hydrophobic core and two hydrophilic ends of the spin radical labeled transmembrane sites. From the $\Phi_{micelle}$, Π_{O2} and Π_{NiEDDA} values, the junction of the hydrophobic core and interfacial head group regions of LDAO micelles were mapped to around V737R1 and K752R1. However, in the report of glycosylation mapping studies of the integrin β_1 subunit in microsomal membranes, the N-terminal membrane border resided approximately at P731, while the C-terminal membrane border resided approximately at I756[43]. In the present study, the correlational accessibility analysis using the Π_{O2}, Π_{NiEDDA} and $\Phi_{micelle}$ values indicated that the hydrophobic core region was between V737R1 and K752R1, which was much shorter than the region defined in glycosylation mapping studies. Because of its small size, molecular oxygen (O_2) can penetrate into the interior region of the detergent micelles; however, the glycosylation mapping assay can only access the sites in direct contact with the aqueous solvent, and not even the interfacial regions defined by polar head groups of LDAO micelles. Therefore, the conjugated Π_{O2} and Π_{NiEDDA} accessibility data provided a more accurate and clear topological analysis of the transmembrane sites of the integrin β_{1a}-TMC in LDAO micelles.

For the sample of integrin β_{1a}-TMC in POPC/POPG liposomes, the results of accessibility analysis of O_2 and NiEDDA are shown in Figure 6a and 6b (red dots), respectively. Since detergent micelles are normally used to mimic the amphipathic liposomes (hydrophobic interior and hydrophilic exterior), we expected a similar Π_{O2} and Π_{NiEDDA} value distribution of integrin β_{1a}-TMC in POPC/POPG liposomes as that observed in detergent micelles. However, the Π_{NiEDDA} values were lower (approximately 0.025) (Fig. 6a, red dots), indicating low hydrophilic accessibility. The Π_{O2} values were not in

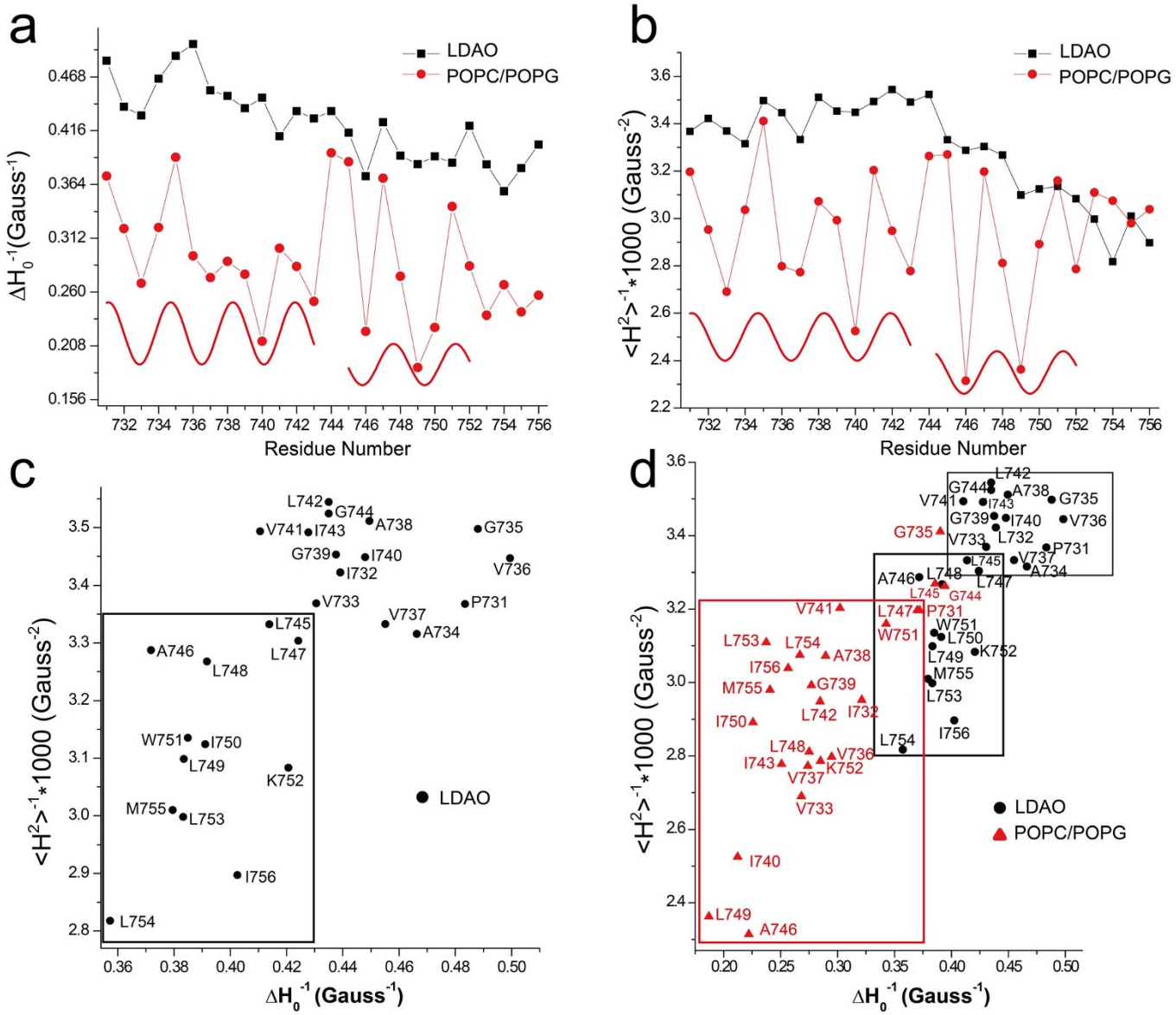

Figure 4 | EPR Mobility analysis of integrin β_{1a}-TMC in LDAO micelles and in POPC/POPG liposomes. (a) Plot of the reciprocal of the central resonance line width ΔH^{-1} versus the residue number in micelles (black squares) and in liposomes (red dots). (b) Plot of the inverse spectral second moment of the EPR spectrum $<H^2>^{-1}$ versus the residue number in LDAO micelles (black squares) and in POPC/POPG liposomes (red dots). Sine waves were drawn to illustrate the observed periodicity of ΔH^{-1} and $<H^2>^{-1}$ indicative of a helical structure in (a) and (b). (c) Correlation diagram of $<H^2>^{-1} \sim \Delta H^{-1}$ of integrin β_{1a}-TMC in LDAO micelles. Two rectangular boxes were drawn to indicate the two different mobility groups. (d) Correlation diagram of $<H^2>^{-1} \sim \Delta H^{-1}$ of integrin β_{1a}-TMC in LDAO micelles (black dots) and in POPC/POPG liposomes (red triangles) were plotted in the same scale to show the difference between the two mediums. A blue box was drawn to include almost all residues while two red boxes were drawn as in (c).

the high range, but showed large fluctuations from 0.1 to 0.5, with an average value of 0.3 (Fig. 6b, red dots). However, the derived $\Phi_{liposome} = \ln[\Pi_{O2}/\ \Pi_{NiEDDA}]$ was relatively high, although it showed large fluctuations. Therefore, the Π_{NiEDDA}, Π_{O2} and $\Phi_{liposome}$ values indicated the relative hydrophobic regions along the primary amino acid sequence of the transmembrane domain of the integrin β_{1a}-TMC in POPC/POPG liposomes. The fluctuations of the Π_{O2} and $\Phi_{liposome}$ values were also fitted using the sine-wave with a period of 3.6, which strongly indicated an α-helical secondary structure (Fig. 6b, 6c). Considering the previous highly immobilized sites in the $\Delta H^{-1} - <H^2>^{-1}$ diagram of the integrin β_{1a}-TMC in POPC/POPG liposomes (Fig. 4d), it is likely that the transmembrane domain of the integrin β_{1a}-TMC formed homo-oligomers through inter-helical interactions. Therefore, the observed low values of Π_{NiEDDA} may have been due to the low solubility of NiEDDA in the hydrophobic inter-helical contacts and the consequent homo-oligomeric clustering effects, and not to the conventional hydrophobic interior environment of liposomes, which would result in a standard distribution as in detergent micelles. The proposed homo-oligomeric clustering of the integrin β_{1a}-TMC was consistent with the observed multiple bands in the SDS-PAGE analysis (Fig. 1c right) of the protein in POPC/POPG liposomes.

Different oligomeric states of the integrin β_{1a}-TMC in micelles or liposomes. As indicated above, the EPR mobility and accessibility analysis of the transmembrane domain of the integrin β_{1a}-TMC in detergent micelles clearly demonstrated a transmembrane helix topology. Moreover, the lack of periodic fluctuation in mobility parameters (ΔH^{-1} and $<H^2>^{-1}$) and accessibility parameters (Π_{NiEDDA}, Π_{O2} and the $\Pi_{micelle}$) indicated that there are only pure

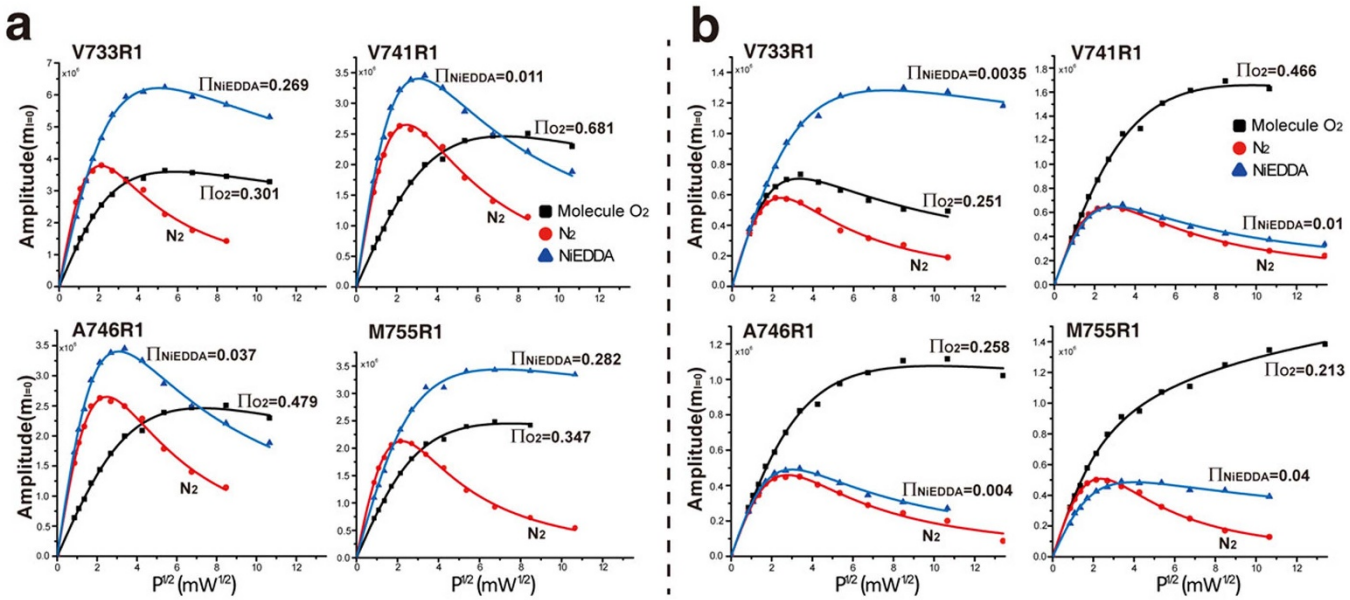

Figure 5 | EPR Power saturation curves for integrin β_{1a}-V733R1, -V741R1, -A746R1 and -M755R1 in LDAO micelles (a) and in POPC/POPG liposomes (b). The power saturation curves were obtained under three conditions: molecular oxygen (O_2), nitrogen (as a control) and the reagent NiEDDA (50 mM). Π_{O2} and Π_{NiEDDA} values from fitting were shown.

interactions between R1 in monomeric proteins and the hydrophobic core or interfacial regions of detergent micelles.

Detergent micelles are considered as good mimics of the native environment of lipid bilayers because detergent micelles can support the native stability, structure, and functionality of membrane proteins[44]. Under this assumption, the mobility and accessibility data of the reconstituted integrin β_{1a}-TMC in POPC/POPG liposomes might follow similar patterns as those obtained in LDAO micelles, provided the protein was also a monomer in liposomes. However, different mobility and accessibility patterns were observed for the integrin β_{1a}-TMC in detergent micelles versus liposomes.

In POPC/POPG liposomes, a stronger overall immobilization of the integrin β_{1a}-TMC was observed in liposomes than in LDAO micelles (Fig. 4d). Distinctive periodicity in the mobility parameters (ΔH^{-1} and $<H^2>^{-1}$) was also observed in liposomes (Fig. 4a, 4b) rather than in LDAO micelles, suggesting the existence of inter-residue tertiary interactions in the sample of integrin β_{1a}-TMC in liposomes, in contrast to the interactions between detergent molecules and transmembrane residues of the monomeric integrin β_{1a}-TMC in LDAO micelles.

The observed different accessibility patterns also suggested different oligomeric states of integrin β_{1a}-TMC in liposomes than in detergent micelles. Overall, similar ascending and descending patterns were observed in detergent micelles and in liposomes, suggesting a similar topology or immersion depth of the transmembrane domain of the integrin β_{1a}-TMC. However, the $\Phi_{liposome}$ showed a larger fluctuation amplitude than the $\Phi_{micelles}$, indicating the presence of hydrophobicity differences between the two samples. Through the accessibility data (including the Π_{O2}, Π_{NiEDDA}, $\Phi_{micelles}$), the center of the monomeric transmembrane domain was clearly identified for the integrin β_{1a}-TMC in detergent micelles (black squares and line in Fig. 6). However, the center of the transmembrane domain was not clear for the clustered integrin β_{1a}-TMC in liposomes (red dots and line in Fig. 6), which was due to the presence of protein-protein interactions (possibly of the leucine-zipper like hydrophobic interactions, Fig. 7b), besides the interactions between the side chains of transmembrane residues of integrin β_{1a}-TMC and hydrophobic acyl-chain, hydrophilic glycerol skeleton, or polar head groups of liposomes. At the same time, very distinctive periodic patterns were observed for Π_{NiEDDA}, Π_{O2} and $\Phi_{liposome}$ values in liposomes but not in detergent micelles (Fig. 6), suggesting the helical conformation (with periodicity of 3.6) and inter-helical interactions of the integrin β_{1a} transmembrane domain in liposomes. The non-periodic patterns of the Π_{NiEDDA}, Π_{O2} and $\Phi_{micelles}$ values in LDAO were possibly due to the solely helix-detergent interactions. Furthermore, similarities in the phase of the period indicated that the O_2 inaccessible residues, including I740R1, A746R1, L749R1, and L753R1 (Fig. 6b), were also the more immobilized residues (Fig. 2, 4a, 4b). Those O_2 inaccessible and immobilized residues might interact with other residues, rather than directly with the hydrophobic tails of lipid molecules. If the inter-helical interactions occurred between two identical proteins, the Leu-Leu, Ala-Ala, Ile-Ile interaction pairs and the period numbers of 3 (749–746), 6(746–740) and 4 (753–749) demonstrated that those residues were lined on the same side of the inter-helical interaction (an ideal helix has a periodic pitch of 3.6 residue), forming a leucine-zipper pattern that is typical of the oligomerization behavior of the transmembrane domains of many membrane proteins[41,45]. A leucine-zipper-like motif was proposed to drive the strong self-association of the transmembrane domain of the discoidin family of receptor tyrosine kinases (DDR1 and DDR2)[46] and the self-assembling erythropoietin receptor transmembrane segments[47].

Discussion

The present EPR mobility and accessibility analysis indicated that the transmembrane domain of the integrin β_{1a}-TMC forms a monomeric helix in LDAO micelles and clusters of homo-oligomeric helices of integrin β_{1a}-TMC in POPC/POPG liposomes. These distinctive environmental influences imply that detergent micelles might not mimic lipid bilayers in high fidelity, especially because of their globular shape and spherical surface, which can only provide space for membrane proteins with a small number of helices. While liposomes provide space for the free lateral motion of membrane proteins, inter-helical interactions may drive the formation of integrin clusters. Tentative models of the integrin β_{1a}-TMC in detergent micelles and liposomes are shown in Figure 7. Briefly, the integrin β_{1a}-TMC adopted a single monomeric helical conformation with a non-helical secondary structure at site G744 (Fig. 7a), whereas the protein formed inter-helical clusters in liposomes (Fig. 7c) with undefined numbers of monomers, consistent with the multiple-bands observed in the SDS-PAGE analysis of samples from lipo-

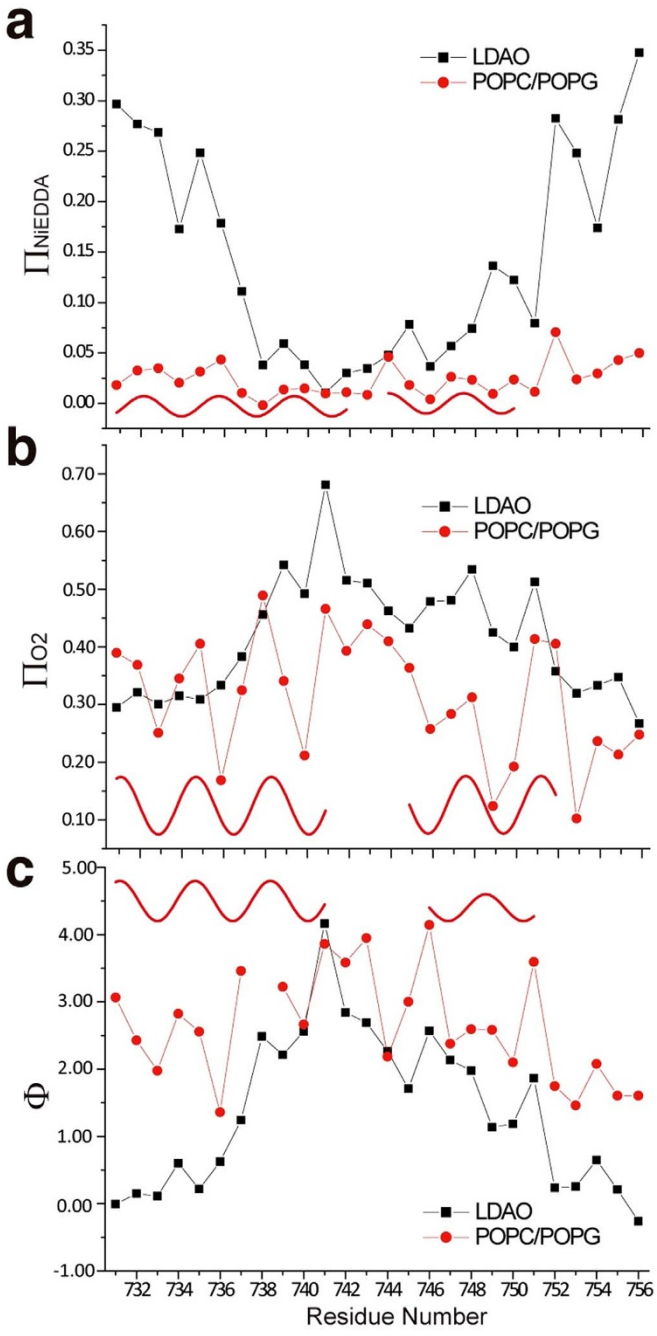

Figure 6 | EPR accessibility analysis of integrin β_{1a}-TMC in LDAO micelles and in POPC/POPG liposomes using power saturation experiments. Residue-specific environmental parameter profiles: NiEDDA accessibility parameter (Π_{NiEDDA}, panel a), oxygen accessibility parameter (Π_{O2}, panel b) and the corresponding depth parameter (Φ, panel c) in LDAO micelles (black squares) and in POPC/POPG liposomes (red dots) were plotted versus the residue number. Sine waves were drawn to illustrate the observed periodicity indicative of a helical structure in POPC/POPG liposomes.

somes (Fig. 1c right). Residues showing low mobility and O_2 accessibility, such as A746R1, L749R1, L753R1 and L754R1, might play an important role in the helix-helix interaction between the transmembrane domains of integrin β_{1a}-TMC, in a way similar as Leucine zipper (Fig. 7b).

The kink G744 was derived from the observed mobility analysis data in detergent micelles. Although both the central line-width ΔH and the second moment $<H^2>$ were used to indicate mobility of the spin labeled site, the central line-width ΔH and the second moment $<H^2>$ are determined primarily by the degree of averaging of the anisotropic g tensors and the anisotropic hyperfine (A) tensor, respectively[39]. Moreover, for sites at which multiple populations of mobility states are observed, the central line-width ΔH is dominated by the most mobile component while the second moment $<H^2>$ is biased toward the immobilized component[39]. Therefore, with the drop of the second moment $<H^2>$ of residues after G744 in the transmembrane domain of integrin β_{1a}-TMC, these residues were more immobilized, probably due to the strong stabilization interactions between hydrophobic side chains of the residues following G744 and the acyl-chain of detergents.

The lateral assembly of integrin clusters during cell adhesion, migration and signaling were found to be essential for cell survival and function in many cell types[12]. Homo- or hetero-oligomeric interactions between the transmembrane helices of integrin α or β subunits may play important roles in integrin activation and clustering[48]. *In vitro* studies have shown that the activation-induced transmembrane domain separation in integrins induces clustering, with the corresponding homo-oligomerization of the α or β transmembrane domains[11,49,50]. Homomeric interactions were observed for transmembrane helices of integrin α_{IIb} in DPC micelles[50], whereas no *in vitro* reports exist describing the homo-oligomeric integrin clusters in liposomes. In the present study, EPR mobility and accessibility analysis demonstrated that the transmembrane domain of the integrin β_{1a}-TMC formed homo-oligomeric clusters in POPC/POPG liposomes resulting from hemophilic interactions between transmembrane helices, similar to the Leucine zipper conformation. Previous studies showed that the lipid bilayer could contribute to transmembrane helix oligomerization[41,51]. The present study demonstrated that phospholipid liposomes can induce and enhance the formation of integrin clusters, providing a more native-like environment for cluster formation in integrin proteins.

Methods

Construction of cysteine mutations in human integrin β_{1a}-TMC. The wild-type oligonucleotides encoding the integrin β_{1a}-TMC (V717-K798) were synthesized by Sangon (Shanghai). The cysteine at site 723 was first mutated to serine by site-directed mutagenesis using the PCR-based overlap extension method. The consequent cys-less sequence was then used as template for further mutagenesis. A total of 26 residues (from P731 to I756) were substituted with cysteine (Fig. 1b). The 26 single-cys mutants were introduced into the plasmid expression vector pET21b (Novagen), which carries a 6 × His-tag at the C-terminus. All mutant constructs were verified by DNA sequencing.

Protein expression and purification. Expression and purification of the integrin β_{1a}-TMC were performed as described for integrin α_{1a}-TMC in a previous report[24]. Briefly, integrin β_{1a}-TMC expression was induced by addition of isopropyl-β-D-thiogalactoside (IPTG) to a final concentration of 0.8 mM in LB medium at a cell density of OD_{600} = 0.8. The inclusion body proteins were firstly solubilized in 0.5% SDS, then processed by detergent exchange to 0.2% LDAO on a Ni^{2+}-NTA column. The proteins were further purified through size exclusion chromatography on a Superdex 200 10/300 GL column (GE healthcare) in a buffer consisting of 20 mM Tris, 100 mM NaCl, 0.2% LDAO, 2 mM DTT, pH 8.0. For proteins that were subsequently reconstituted into POPC/POPG liposomes, 0.2% LDAO was substituted by 0.2% (w/v) DM (n-decyl-β-D-maltopyranoside, Anatrace) during size exclusion chromatography. The concentration of the purified protein was determined by OD_{280}, and the purity was analyzed by sodium dodecyl sulfate polyacrylamide gel electrophoresis (SDS-PAGE). All mutants were at least 95% pure according to SDS-PAGE. All samples were boiled in SDS-PAGE loading buffer for 10 minutes to totally denature the protein before loading onto gels.

Site specific spin radical MTSL labeling. Prior to spin labeling, DTT was removed using a PD-10 gravity flow desalting column (GE Biosciences), eluting with binding buffer (20 mM Tris, 100 mM NaCl, pH 8.0) in the presence of 0.2% (w/v) LDAO. Single cysteine mutants were immediately reacted with a 10-fold molar excess of spin radical MTSL (R1: 1-oxyl-2,2,5,5-tetramethyl-Δ3-pyrr-oline-3-methyl methanethiosulfonate, Toronto Research Chemicals, Ontario, Canada) at room temperature for 30 min and then at 4°C overnight. Excessive spin reagents were removed through gel filtration chromatography in binding buffer with 0.2% LDAO (0.2% DM for samples which were subsequently reconstituted into POPC/POPG liposome). For samples in LDAO micelles, Amicon Ultra-15 centrifugal filter units (Millipore) were used to concentrate the sample to a final concentration of approximately 200 uM. The spin-labeled samples in LDAO micelles were

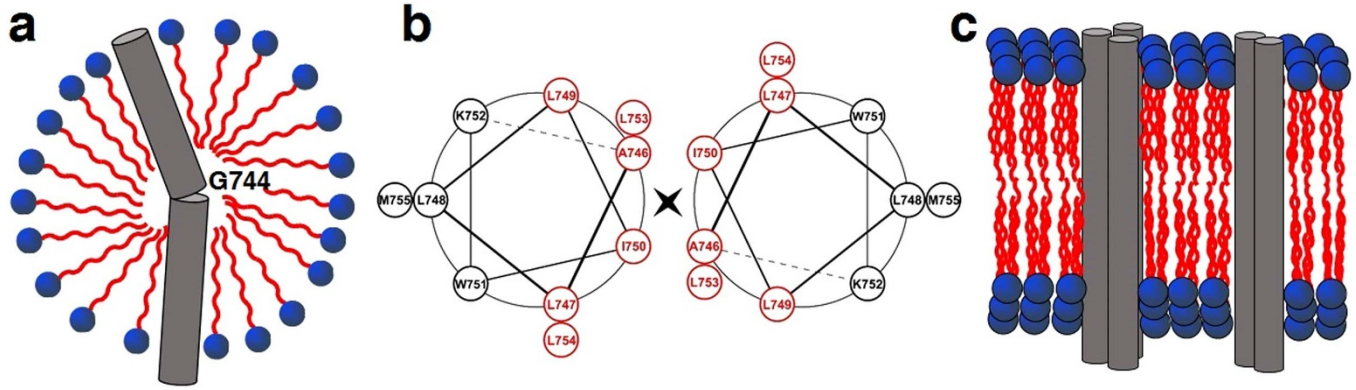

Figure 7 | Schematic models of the integrin β_{1a}-TMC in detergent micelles or in liposomes. (a) The transmembrane domain of integrin β_{1a}-TMC adopted a monomeric helix with a kink at residue G744. (b) Helical wheel diagram depicting the interface between the hydrophobic side chains of residues in the transmembrane domain (Ala746-Met755) of integrin β_{1a}-TMC. Residues which might be involved in forming the hydrophobic interactions were colored in red. (c) Homo-oligomeric transmembrane domains of integrin β_{1a}-TMC in liposomes. The clustering effect of transmembrane helices was represented by the formation of inter-helical dimers and trimers. The extracellular domain and cytoplasmic tail were eliminated for simplicity. Red areas represent the hydrophobic tail, and blue areas are the hydrophilic head for the illustration of detergent and phospholipid molecules.

subsequently used for CW-EPR and power saturation EPR experiments. Labeling efficiency was determined by measuring the protein concentration and the spin concentration. As determined by double integration of the EPR spectra, the labeling efficiency for each mutant was beyond 90%. Spin labeled integrin β_{1a}-TMC was designated by giving the single letter code for the original residue, the sequence number, and the letter code "R1" for the introduced spin label (e.g. L742R1 means the R1 introduced at Leu742 site).

Reconstitution into POPC/POPG Liposomes. Powders of POPC (1-palmitoyl-2-oleoyl-sn-glycero-3-phosphocholine) and POPG (1-palmitoyl-2-oleoyl-sn-glycero-3-phospho-(1′-rac-glycerol) (sodium salt), Avanti, Alabaster, AL) were mixed in chloroform (3 : 1 POPC : POPG molar ratio). The solution was gently dried under a nitrogen flow and then placed under a high vacuum overnight to further evaporate any residual solvent. The lipid film was rehydrated with binding buffer to yield a final concentration of approximately 4 mg/ml, and dispersed through vigorous stirring followed by at least 10 rounds of freeze−thaw−sonication until a clear solution was obtained. The resulting solution was filtered 20 times through a 100 nm polycarbonate membrane filter (Whatman, Newton, MA) mounted on a mini-extruder. The spin-labeled integrin β_{1a}-TMC (in binding buffer with 0.2% DM) and the extruded phospholipid liposomes were mixed to obtain a lipid/protein molar ratio of 200 : 1. Two cycles of freeze−thaw−sonication were performed to improve the even distribution of integrin β_{1a}-TMC in liposomes. Membrane protein reconstitution was implemented by dialysis against 200-fold excessive binding buffer for a total of 48 h, with buffer changes every 12 h. After dialysis, the proteoliposome samples were pelleted down by ultracentrifugation at 300,000 g for 30 min. The pellet was then thoroughly re-suspended in binding buffer and extruded through the 100 nm filter again to obtain homogeneous protein-incorporated vesicles in the size range of 50–100 nm. The reconstituted spin-labeled samples in POPC/POPG liposomes were subsequently used for CW-EPR measurements and power saturation EPR experiments.

Circular dichroism (CD) spectroscopy analysis. Integrin β_{1a}-L749R1 in LDAO micelles was diluted to 0.10 mM in 50 mM NaH_2PO_4–Na_2HPO_4 buffer, pH 8.0. CD measurements were performed on a Jasco-810 spectropolarimeter at 298 K. CD spectra were recorded over a wavelength range of 190–280 nm using a cuvette of 1-mm path length at a scanning speed of 20 nm/min and subjected to 10 scans. Acquired data were normalized by subtracting the baseline recorded for the buffer only and are shown in the supplementary data (Supplementary. Fig. S2). The acquired CD spectra of integrin β_{1a}-L749R1 in LDAO micelles were used for secondary structure estimation using a curve-fitting method[52]. CD spectroscopy was not performed for samples in liposomes because of the strong perturbations in the CD signal due to depolarization caused by light scattering[53,54].

Continuous wave EPR spectroscopy. CW-EPR spectroscopy was performed on a Bruker A300 spectrometer (Bruker Biospin GmbH, Rheinstetten, Germany) at X-band (9.5 GHz) equipped with a high-sensitivity cavity (ER 4119HS, Bruker Biospin GmbH, Rheinstetten, Germany) at room temperature (298 K). Spectra were recorded at a microwave power of 2 mW over a scan width of 200 Gauss with a field modulation of 1 Gauss at a frequency of 100 kHz. Samples were placed in a glass capillary tube in a volume of approximately 20 μL. Data acquisition was performed 20–40 times to achieve a reasonable signal/noise ratio.

Rotational correlation time (τ_c) and mobility parameter calculation. The rotational correlation time (τ_c) of spin labeled integrin β_{1a}-TMC in detergent micelles and in liposomes was estimated as described previously[37,38]. Briefly, continuous wave EPR spectra of the spin labeled protein in detergent micelles and in liposomes were acquired under two thermal conditions: at ambient temperature (298 K) and at its rigid limit (frozen solution at 150 K, data not shown). The rotational correlation time τ_c was evaluated from the expression,

$$\tau_c = a(1-S)^b \tag{1}$$

where

$$S = A'_{zz}(G)/A^R_{zz}(G) \tag{2}$$

A^R_{zz} is identical to the magnetic tensor A_{zz} and A'_{zz} is the generic room-temperature genera magnetic tensor[37,38]. The values of $a = 8.52 \times 10^{-10}$ sec and $b = -1.16 \times 10^{-10}$ sec are determined by evaluating the peak-to-peak derivative Lorentzian linewidth (δ) derived from the rigid limit EPR spectrum.

The inverse line width of the central $m_{I=0}$ resonance line (ΔH^{-1}) and the inverse spectral second moment ($<H^2>^{-1}$) were analyzed to further extract information on the mobility of the integrin β_{1a}-TMC in detergent micelles and in liposomes. The second moment of spectra was calculated to represent the spectral breadth:

$$\langle H^2 \rangle = \frac{\int (B - \langle H \rangle)^2 S(B) dB}{\int S(B) dB} \tag{3}$$

which is defined based on the first moment <H> (the mean or geometrical center of the spectrum):

$$\langle H \rangle = \frac{\int BS(B) dB}{\int S(B) dB} \tag{4}$$

where B is the magnetic field, and S(B) is the absorption spectrum of the spin-labeled protein[39].

EPR power saturation studies and accessibility analysis. Power saturation experiments were performed on the same spectrometer coupled with an ER4123D CW resonator (Bruker BioSpin). Samples were loaded into gas permeable TPX capillary tubes with a total volume of 3–4 μL at a concentration of 50–100 μM. EPR data were collected using a modulation amplitude of 1 Gauss and a scan range of 15 Gauss. The range of the incident microwave power was 0.7 to 180 mW for power saturation experiments. Nitrogen was used as a control to purge oxygen and other paramagnetic relaxing reagents in the sample. The water-soluble paramagnetic reagent, Nickel(II)-EDDA complex (NiEDDA) was synthesized as previously described[33]. The power saturation curves were obtained for integrin β_{1a}-TMC in LDAO micelles and POPC/POPG liposomes under three conditions: (1) equilibrated with the hydrophobic paramagnetic reagent 21% O_2 (air), (2) equilibrated with nitrogen as a control, and (3) equilibrated with nitrogen in the presence of the hydrophilic paramagnetic reagent NiEDDA (50 mM).

Power saturation curves were measured and the accessibility parameters Π_{O2} and Π_{NiEDDA} were derived from fitting the saturation curves[33]. Briefly, the saturation curves were measured as the vertical peak-to-peak amplitude (A) of the first derivative $M_i = 0$ line as a function of incident microwave power (P)[33]. The data points were then fit using an R software script according to equation (5):

$$A = I\sqrt{P}[1 + (2^{1/\varepsilon} - 1)P/P_{1/2}]^{-\varepsilon} \tag{5}$$

where I is a scaling factor, $P_{1/2}$ is the power where the first derivative amplitude is reduced to half of its unsaturated value, and ε is a measure of the homogeneity of

saturation of the resonance line. The change in $P_{1/2}$, $\Delta P_{1/2}$, is calculated as the difference in $P_{1/2}$ values in the presence and absence of relaxing agent. The parameter $\Delta P_{1/2}/\Delta H_{pp}$ is normalized to the same parameter for a reference sample to account for instrumental variations, where ΔH_{pp} is the peak-to-peak line-width of the first derivative spectrum. The corresponding accessibility parameter, Π, is calculated using the following equation:

$$\Pi = \{\Delta P_{1/2}/\Delta H_{pp}\}/\{P_{1/2}(DPPH)/\Delta H_{pp}(DPPH)\} \quad (6)$$

where $P_{1/2}$ (DPPH) and ΔH_{pp} (DPPH) are the $P_{1/2}$ and line-width values determined for a standard sample of crystalline 2,2-diphenyl-1-picrylhydrazyl (DPPH) in KCl[33].

1. Hynes, R. O. Integrins: bidirectional, allosteric signaling machines. *Cell* **110**, 673–687 (2002).
2. Ginsberg, M. H., Partridge, A. & Shattil, S. J. Integrin regulation. *Curr Opin Cell Biol* **17**, 509–516 (2005).
3. Vinogradova, O. *et al.* A structural mechanism of integrin alpha(IIb)beta(3) "inside-out" activation as regulated by its cytoplasmic face. *Cell* **110**, 587–597 (2002).
4. Hynes, R. O. Targeted mutations in cell adhesion genes: what have we learned from them? *Dev Biol* **180**, 402–412 (1996).
5. Luo, B. H., Springer, T. A. & Takagi, J. A specific interface between integrin transmembrane helices and affinity for ligand. *PLoS Biol* **2**, e153 (2004).
6. Partridge, A. W., Liu, S., Kim, S., Bowie, J. U. & Ginsberg, M. H. Transmembrane domain helix packing stabilizes integrin alphaIIbbeta3 in the low affinity state. *J Biol Chem* **280**, 7294–7300 (2005).
7. Lau, T. L., Dua, V. & Ulmer, T. S. Structure of the integrin alphaIIb transmembrane segment. *J Biol Chem* **283**, 16162–16168 (2008).
8. Hughes, P. E. *et al.* Breaking the integrin hinge. A defined structural constraint regulates integrin signaling. *J Biol Chem* **271**, 6571–6574 (1996).
9. Li, W. *et al.* A push-pull mechanism for regulating integrin function. *Proc Natl Acad Sci U S A* **102**, 1424–1429 (2005).
10. Luo, B. H., Carman, C. V., Takagi, J. & Springer, T. A. Disrupting integrin transmembrane domain heterodimerization increases ligand binding affinity, not valency or clustering. *Proc Natl Acad Sci U S A* **102**, 3679–3684 (2005).
11. Li, R. *et al.* Activation of integrin alphaIIbbeta3 by modulation of transmembrane helix associations. *Science* **300**, 795–798 (2003).
12. Welf, E. S., Naik, U. P. & Ogunnaike, B. A. A spatial model for integrin clustering as a result of feedback between integrin activation and integrin binding. *Biophys J* **103**, 1379–1389 (2012).
13. Miyamoto, S. *et al.* Integrin function: molecular hierarchies of cytoskeletal and signaling molecules. *J Cell Biol* **131**, 791–805 (1995).
14. Hynes, R. O. Integrins: versatility, modulation, and signaling in cell adhesion. *Cell* **69**, 11–25 (1992).
15. Anthis, N. J. & Campbell, I. D. The tail of integrin activation. *Trends Biochem Sci* **36**, 191–198 (2011).
16. Gardner, H. A. Integrin signaling in fibrosis and scleroderma. *Curr Rheumatol Rep* **1**, 28–33 (1999).
17. Pozzi, A. *et al.* Elevated matrix metalloprotease and angiostatin levels in integrin alpha 1 knockout mice cause reduced tumor vascularization. *Proc Natl Acad Sci U S A* **97**, 2202–2207 (2000).
18. Ekholm, E. *et al.* Diminished callus size and cartilage synthesis in alpha 1 beta 1 integrin-deficient mice during bone fracture healing. *Am J Pathol* **160**, 1779–1785 (2002).
19. McBrien, N. A., Metlapally, R., Jobling, A. I. & Gentle, A. Expression of collagen-binding integrin receptors in the mammalian sclera and their regulation during the development of myopia. *Invest Ophthalmol Vis Sci* **47**, 4674–4682 (2006).
20. Rentala, S., Yalavarthy, P. D. & Mangamoori, L. N. Alpha1 and beta1 integrins enhance the homing and differentiation of cultured prostate cancer stem cells. *Asian J Androl* **12**, 548–555 (2010).
21. Tamkun, J. W. *et al.* Structure of integrin, a glycoprotein involved in the transmembrane linkage between fibronectin and actin. *Cell* **46**, 271–282 (1986).
22. Fitzgerald, L. A., Steiner, B., Rall, S. C., Jr., Lo, S. S. & Phillips, D. R. Protein sequence of endothelial glycoprotein IIIa derived from a cDNA clone. Identity with platelet glycoprotein IIIa and similarity to "integrin" *J Biol Chem* **262**, 3936–3939 (1987).
23. Anthis, N. J. *et al.* The structure of an integrin/talin complex reveals the basis of inside-out signal transduction. *EMBO J* **28**, 3623–3632 (2009).
24. Lai, C., Liu, X., Tian, C. & Wu, F. Integrin alpha1 has a long helix, extending from the transmembrane region to the cytoplasmic tail in detergent micelles. *PLoS One* **8**, e62954 (2013).
25. Lau, T. L., Kim, C., Ginsberg, M. H. & Ulmer, T. S. The structure of the integrin alphaIIbbeta3 transmembrane complex explains integrin transmembrane signalling. *EMBO J* **28**, 1351–1361 (2009).
26. Lau, T. L., Partridge, A. W., Ginsberg, M. H. & Ulmer, T. S. Structure of the integrin beta3 transmembrane segment in phospholipid bicelles and detergent micelles. *Biochemistry* **47**, 4008–4016 (2008).
27. Bordignon, E. & Polyhach, Y. H. EPR techniques to probe insertion and conformation of spin-labeled proteins in lipid bilayers. *Methods Mol Biol* **974**, 329–355 (2013).
28. Smirnova, I. *et al.* Sugar binding induces an outward facing conformation of LacY. *Proc Natl Acad Sci U S A* **104**, 16504–16509 (2007).
29. Yu, L. *et al.* Distance measurement between two flexible sites in proteins in high viscosity medium at physiological temperature using continuous wave EPR. *Protein Cell* **5**, 334–337 (2014).
30. Bordignon, E. Site-directed spin labeling of membrane proteins. *Top Curr Chem* **321**, 121-157 (2012).
31. Howell, S. C., Mesleh, M. F. & Opella, S. J. NMR structure determination of a membrane protein with two transmembrane helices in micelles: MerF of the bacterial mercury detoxification system. *Biochemistry* **44**, 5196–5206 (2005).
32. Long, S. B., Tao, X., Campbell, E. B. & MacKinnon, R. Atomic structure of a voltage-dependent K+ channel in a lipid membrane-like environment. *Nature* **450**, 376–382 (2007).
33. Altenbach, C., Greenhalgh, D. A., Khorana, H. G. & Hubbell, W. L. A collision gradient method to determine the immersion depth of nitroxides in lipid bilayers: application to spin-labeled mutants of bacteriorhodopsin. *Proc Natl Acad Sci U S A* **91**, 1667–1671 (1994).
34. Rath, A., Glibowicka, M., Nadeau, V. G., Chen, G. & Deber, C. M. Detergent binding explains anomalous SDS-PAGE migration of membrane proteins. *Proc Natl Acad Sci U S A* **106**, 1760–1765 (2009).
35. Bendas, G. & Borsig, L. Cancer cell adhesion and metastasis: selectins, integrins, and the inhibitory potential of heparins. *Int J Cell Biol* **2012**, 676731 (2012).
36. Huttenlocher, A. & Horwitz, A. R. Integrins in cell migration. *Cold Spring Harb Perspect Biol* **3**, a005074 (2011).
37. Oppenheim, S. F., Buettner, G. R. & Rodgers, V. G. J. Relationship of rotational correlation time from EPR spectroscopy and protein-membrane interaction. *J Memb Sci* **118**, 133–139 (1996).
38. Goldman, S. A., Bruno, G. V. & Freed, J. H. Estimating slow-motional rotational correlation times for nitroxides by electron spin resonance. *J Phys Chem* **76**, 1858–1860 (1972).
39. McHaourab, H. S., Lietzow, M. A., Hideg, K. & Hubbell, W. L. Motion of spin-labeled side chains in T4 lysozyme. Correlation with protein structure and dynamics. *Biochemistry* **35**, 7692–7704 (1996).
40. Zhou, Z. *et al.* Solution structure of the cytoplasmic domain of erythrocyte membrane band 3 determined by site-directed spin labeling. *Biochemistry* **44**, 15115–15128 (2005).
41. Li, E., Wimley, W. C. & Hristova, K. Transmembrane helix dimerization: beyond the search for sequence motifs. *Biochim Biophys Acta* **1818**, 183–193 (2012).
42. Gurezka, R. & Langosch, D. In vitro selection of membrane-spanning leucine zipper protein-protein interaction motifs using POSSYCCAT. *J Biol Chem* **276**, 45580–45587 (2001).
43. Armulik, A., Velling, T. & Johansson, S. The integrin beta1 subunit transmembrane domain regulates phosphatidylinositol 3-kinase-dependent tyrosine phosphorylation of Crk-associated substrate. *Mol Biol Cell* **15**, 2558–2567 (2004).
44. Coey, A. T. *et al.* Reconstitution of KCNE1 into lipid bilayers: comparing the structural, dynamic, and activity differences in micelle and vesicle environments. *Biochemistry* **50**, 10851–10859 (2011).
45. Oates, J., King, G. & Dixon, A. M. Strong oligomerization behavior of PDGFbeta receptor transmembrane domain and its regulation by the juxtamembrane regions. *Biochim Biophys Acta* **1798**, 605–615 (2010).
46. Noordeen, N. A., Carafoli, F., Hohenester, E., Horton, M. A. & Leitinger, B. A transmembrane leucine zipper is required for activation of the dimeric receptor tyrosine kinase DDR1. *J Biol Chem* **281**, 22744–22751 (2006).
47. Ruan, W., Becker, V., Klingmuller, U. & Langosch, D. The interface between self-assembling erythropoietin receptor transmembrane segments corresponds to a membrane-spanning leucine zipper. *J Biol Chem* **279**, 3273–3279 (2004).
48. Li, R. *et al.* Dimerization of the transmembrane domain of Integrin alphaIIb subunit in cell membranes. *J Biol Chem* **279**, 26666–26673 (2004).
49. Cluzel, C. *et al.* The mechanisms and dynamics of (alpha)v(beta)3 integrin clustering in living cells. *J Cell Biol* **171**, 383–392 (2005).
50. Li, R. *et al.* Oligomerization of the integrin alphaIIbbeta3: roles of the transmembrane and cytoplasmic domains. *Proc Natl Acad Sci U S A* **98**, 12462–12467 (2001).
51. Mokrab, Y., Stevens, T. J. & Mizuguchi, K. Lipophobicity and the residue environments of the transmembrane alpha-helical bundle. *Proteins* **74**, 32–49 (2009).
52. Chang, C. T., Wu, C. S. & Yang, J. T. Circular dichroic analysis of protein conformation: inclusion of the beta-turns. *Anal Biochem* **91**, 13–31 (1978).
53. Mao, D. & Wallace, B. A. Differential light scattering and absorption flattening optical effects are minimal in the circular dichroism spectra of small unilamellar vesicles. *Biochemistry* **23**, 2667–2673 (1984).
54. Persson, D., Thoren, P. E. & Norden, B. Penetratin-induced aggregation and subsequent dissociation of negatively charged phospholipid vesicles. *FEBS Lett* **505**, 307–312 (2001).

Acknowledgments

This work was supported by funds from the Ministry of Science and Technology of China (Grant numbers 2011CB911104 and 2013CB910202), and Projects U1332138 and 31100847 of the National Natural Science Foundation of China.

Author contributions

L.Y., W.W., Yi.X. and C.T. designed the experiments, Ya.X. and Sh.L. made the mutations, Sa.L., C.L. and L.X. expressed the proteins, L.Y. and W.W. made the radical labeling and EPR measurements, L.Y., L.Z. and C.T. analyzed the data and wrote the paper. All authors reviewed the manuscript.

Additional information

Supplementary information accompanies this paper at http://www.nature.com/scientificreports

Competing financial interests: The authors declare no competing financial interests.

How to cite this article: Yu, L. *et al*. CW-EPR studies revealed different motional properties and oligomeric states of the integrin β_{1a} transmembrane domain in detergent micelles or liposomes. *Sci. Rep.* **5**, 7848; DOI:10.1038/srep07848 (2015).